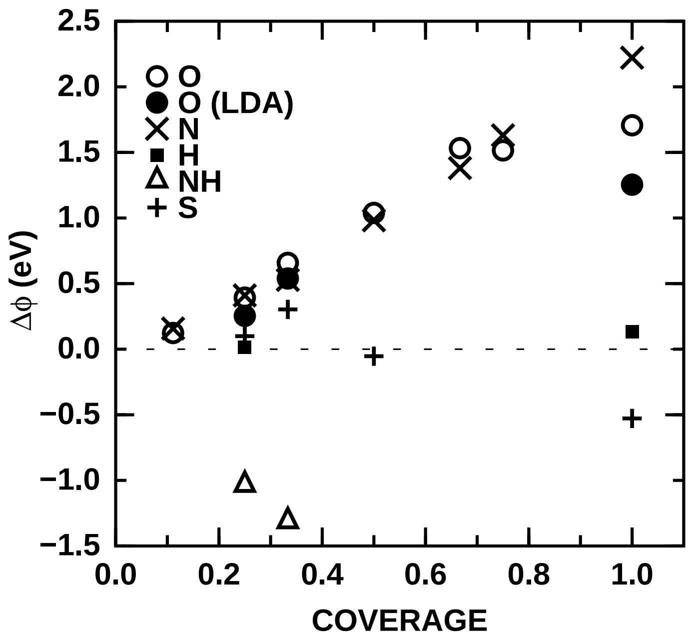

Figure 3.81: The change in work function upon adsorption on Ru (0001) for several electro-negative species; oxygen has been calculated both with the local density and generalised gradient approximations, all the other calculations (Ari P Seitsonen, unpublished results) were done employing the generalised gradient approximation

coverage the change for oxygen levels off but continues for nitrogen.

3.4 Co-adsorption on Ru (0001)

As mentioned in the Introduction the co-adsorption is extremely important since in the Langmuir-Hinshelwood mechanism of the catalytic reaction the reactants, in addition to the possible promoters and inhibitors, adsorb to the surface prior to the reaction. A recent review which covers the structural and electronical aspects of co-adsorption has been published by Herbert Over (1998). Here we shall present our calculated results for three different co-adsorption system where two of the adsorbates of the previous Section, cesium, carbon monoxide and oxygen, are combined at the Ru (0001) surface at a time. This gives us an opportunity to monitor the changes on the adsorbates when they are exposed to a chemically different species on the surface; also the important reactants and test molecule carbon monoxide is combined with the electro-positive cesium and the electro-negative oxygen, which is also the other reactants in the oxidation process of the CO.

3.4.1 Co-adsorption of cesium and oxygen

The co-adsorption of alkali and oxygen atoms has been widely studied (Surnev, 1989). One interesting occurrence of the system is in the ammonia catalysts as discussed *e.g.* by Ertl (1991). On Ru (0001) the co-adsorbed cesium and oxygen has been the subject of studies employing the low energy electron diffraction (Over *et al*, 1992a; Bludau *et al*, 1995; Trost, Wintterlin & Ertl, 1995), scanning tunnelling microscope (Trost, 1995; Trost, Wintterlin & Ertl, 1995) and high-resolution electron energy loss spectroscopy (Jacobi *et al*, 1995). With cesium as very electro-positive and oxygen electro-negative atom the interaction between them is attractive but the repulsion between like

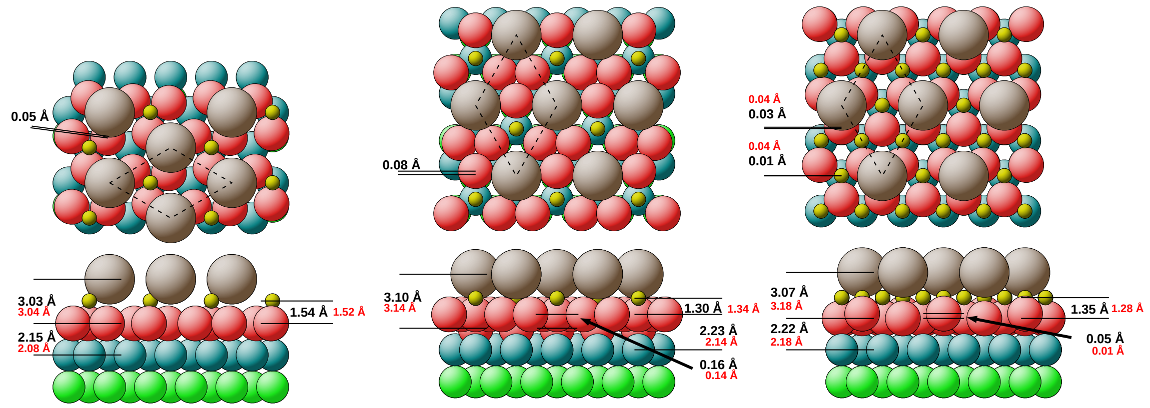

Figure 3.82: The geometries of the Ru (0001)-($\sqrt{3}\times\sqrt{3}$)R30°-(1Cs+1O), Ru (0001)-(2×2)-(1Cs+1O) and Ru (0001)-(2×2)-(1Cs+3O) structures and the separated adsorption structures as obtained from our density functional calculation and the low energy electron diffraction measurements of Over *et al* (1992a) and Kim *et al* (1998); the experimental values are shown with a smaller font

atoms makes the O-Cs-Ru (0001) phase diagram versatile as found by Bludau *et al* (1995); the most abundant phases are arranged into the ($\sqrt{7}\times\sqrt{7}$)R19.1°, ($3\times2\sqrt{3}$) and ($\sqrt{3}\times\sqrt{3}$)R30° unit cells. It is was not until recently that an ordered structure (2×2) with both the cesium and oxygen coverage 1/4 was found (Over, personal communication); however this phase might be only meta-stable against re-ordering into the ($\sqrt{39}\times\sqrt{39}$)R16.1° structure. This is peculiar since both atoms alone form this phase. The cesium-to-oxygen ratio 1:2 corresponds to the existing bulk oxide CsO_2, and structural models close to the (010) face was proposed in the ($3\times2\sqrt{3}$)rect and ($\sqrt{7}\times\sqrt{7}$)R19.1° unit cells.

Trost, Wintterlin and Ertl (1995) studied the phase ordering of the cesium-oxygen "liquid"; in particular they observed the evolution and interplay between the ($\sqrt{7}\times\sqrt{7}$)R19.1° structure and the dis-ordered phase. Jacobi *et al* (1995) studied the re-appearance of the Cs-Ru vibrational mode upon adsorption of different gases; it was found that also oxygen, dissociating readily to atomic species, makes the Cs-Ru mode visible at the cesium coverages larger than 0.22 where the loss became undetectable due to the metallisation of the cesium layer. The co-adsorbed oxygen probably causes a localisation of the electronic states arising from cesium and thus a de-metallisation and subsequently the re-appearance of the energy loss in the spectra.

We performed density functional calculations for the structures Ru (0001)-($\sqrt{3}\times\sqrt{3}$)R30°-(1Cs+1O), Ru (0001)-(2×2)-(1Cs+1O) and Ru (0001)-(2×2)-(1Cs+3O) only due to the larger unit cells and less well known atomic structure in the other configurations. The atoms were placed at the hcp sites in the ($\sqrt{3}\times\sqrt{3}$)R30°-(1Cs+1O) and (2×2)-(1Cs+3O) structures and the oxygen at the hcp and cesium on-top sites in the (2×2)-(1Cs+1O) arrangement, as found in the low energy energy diffraction studies by Over *et al* (1992a; Kim *et al*, 1998). Please note that while cesium adsorbs exactly on the hcp site in the coverage 1/3 the corresponding oxygen-only phase would be unstable towards island formation to domains of (2×2) and (2×1) structures as was discussed in Section 3.3.4. The resulting geometry is shown in the Figure 3.82 with the results from the low energy electron diffraction measurements by Over *et al* (1992a) and listed in the Table 3.21 together with the separated phases.

The most remarkable effect in the co-adsorption geometry is the short Cs-Ru and longer O-Ru distance compared to the separated phases; this is a consequence of the change in the height of

Table 3.21: The adsorption energy, change in work function, layer distances and distance of cesium, cesium and oxygen, and oxygen adsorbed on Ru (0001) in the $(\sqrt{3}\times\sqrt{3})$R30°-(1Cs+1O) structure from our density functional calculations. E_{ads,O_2} is the adsorption energy relative to the oxygen dimer, E_{ads} the mixing energy from the separated $(\sqrt{3}\times\sqrt{3})$R30°-Cs and $(\sqrt{3}\times\sqrt{3})$R30°-O phases

	Cs/Ru	O/Cs/Ru	O/Ru
E_{ads,O_2} (eV)	—	3.19	2.81
E_{mix} (eV)	—	0.37	—
$\Delta\phi$ (eV)	−3.24	−3.36	+0.66
d_{Cs-Ru} (Å)	3.50	3.45	—
d_{O-Ru} (Å)	—	2.19	2.07
d_{12} (Å)	2.15	2.15	2.16
z_{Cs-Ru} (Å)	3.09	3.03	—
z_{O-Ru} (Å)	—	1.54	1.29
Δx (Å)	+0.05	+0.05	+0.02

the atoms since the lateral relaxation – and the first interlayer distance d_{12} – are hardly affected. The same trend was found in the low energy energy diffraction measurements of Over *et al* (1992a), although the reduction in the height z_{Cs-Ru} is larger in the experiments, −0.11 Å; however, in the structure $(\sqrt{3}\times\sqrt{3})$R30°-Cs the distance was too small in the calculations, maybe due to the neglect of zero-point and thermal vibrations which are probably diminished in the more tightly packed co-adsorbed phase. Except for the layer distance d_{12} the experimental and theoretical geometries agree extremely well.

From the energies we see that the mixing of the cesium and oxygen layers stabilises both atoms compared to the separated phases by 0.37 eV. However, the $(\sqrt{3}\times\sqrt{3})$R30°-O would not be stable without cesium and we estimate from the (2×2)-O and (2×1)-O structures in the Figure 3.80 that the oxygen phase $(\sqrt{3}\times\sqrt{3})$R30°-O would have to be bound by 2.91 eV in order to be the preferred structure at the oxygen coverage 1/3, *i.e.* in order to prevent formation of domains. Therefore the real mixing energy of the combined cesium-oxygen phase is actually 0.28 eV, compared to the separated phases; thus the formation of the mixed phase is still rather favourable but this does not imply that islands of $(\sqrt{3}\times\sqrt{3})$R30°-(1Cs+1O) would be formed, even at concentration ratio 1:1, since the other structures with coverages different from 1/3 can be more stable. We have no access to the full phase diagram from our density functional calculations until many more unit cells and structures have been studied.

The work function in the mixed phase is lowered even from the pure cesium structure. This could be expected based on the geometry where the oxygen layer is below the cesium atoms and the cesium is closer to the first ruthenium layer in the mixed phase. All this agrees (Over *et al*, 1992a) with the model of the cesium denoting charge to the oxygen, fitting well to the electro-positivity of cesium and electro-negativity of oxygen; however it also could be explained from interaction between the cesium and oxygen, leading to a reduction in the layer distance between them. To obtain insight to this question we show the density difference in the structure (2×2)-(1Cs+1O) in the Figure 3.83. The change around the cesium atom is very small, whereas around the oxygen and ruthenium atoms there appears a polarisation, which for the oxygen can be qualitatively represent like the change in the Figure 3.84. Please notice that the largest change in the magnitude appears in the

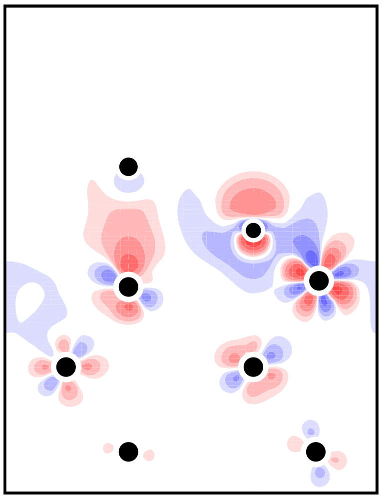

Figure 3.83: The change in the electron density due to the co-adsorption of cesium and oxygen to form the (2×2)-(1Cs+1O) structure

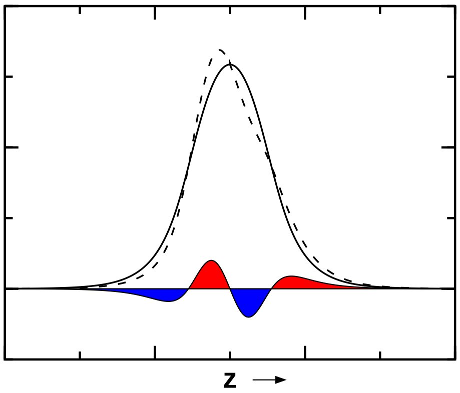

Figure 3.84: A schematic illustration of the change in the electron density on the vertical line passing through the centre of the oxygen atom due to the co-adsorption of cesium and oxygen to form the (2×2)-(1Cs+1O) structure

core region.

We further compare our results to the experimental images produced by the scanning tunnelling microscope; the measurements are from Trost (1995; Trost, Wintterlin & Ertl, 1995). In the Figures 3.85 and 3.86 we show the height maps of the constant density *i. e.* of a constant current within the Tersoff-Hamann model. The value of the density was chosen so that it reproduced the maximal corrugation from the experiments along a cut through the adsorbates. The Figure 3.87 can be compared to the measured images in the work of Trost (1995); the agreement is very good in both cases.

3.4.2 Co-adsorption of cesium and carbon monoxide

Also the co-adsorbed alkali metal and carbon monoxide mutually stabilise each other as was found in the thermal desorption spectroscopy for example in the case of K and CO on Ni (110) (Brodén, Gafner & Bonzel, 1979), Na, K and Cs with CO on Ni (100) (Kiskinova, 1981), and K and CO on Ru (0001) (Madey & Benndorf, 1985); an example of the thermal desorption spectra (Over *et al*, 1995b) is shown in the Figure 3.88 for Cs and CO on Ru (0001): whereas the desorption of Cs alone begins already at 450 K and the one of CO at 350 K, in the co-adsorbed layer the desorption does

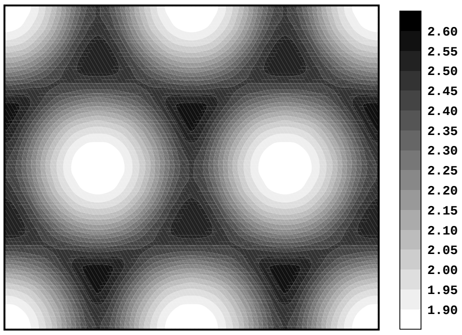

Figure 3.85: A pseudo scanning tunnelling microscope image from the Tersoff-Hamann model in the (2×2)-(1Cs+1O) structure

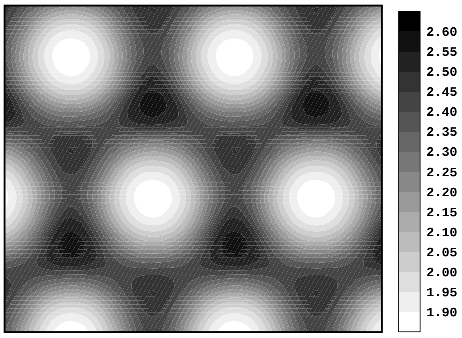

Figure 3.86: A pseudo scanning tunnelling microscope image from the Tersoff-Hamann model in the $(\sqrt{3} \times \sqrt{3})R30°$-(1Cs+1O) structure

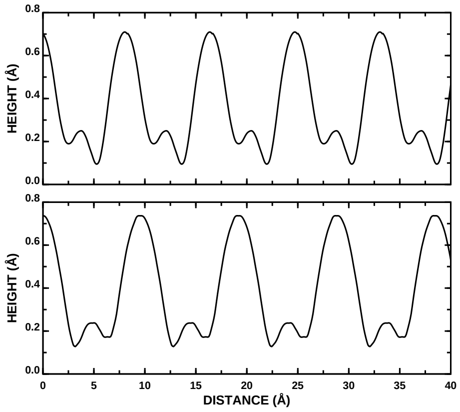

Figure 3.87: A cut through the pseudo scanning tunnelling microscope image from the Tersoff-Hamann model in the $(\sqrt{3} \times \sqrt{3})R30°$-(1Cs+1O) – upper panel – and (2×2)-(1Cs+1O) – lower panel – structures